16th International Symposium on Particle Image Velocimetry – ISPIV 2025
June 26–28, 2025, Tokyo, Japan

Characterization of the Transonic Flow in a Turbine Cascade using High-speed PIV

M. Schroll[1,*], J. Klinner[1,*], C. Willert[1,*], A. Petersen[2], R. Brakmann[2]

[1] Engine Measurement Techniques, DLR Institute of Propulsion Technology, Deutsches Zentrum für Luft- und Raumfahrt (German Aerospace Center), Köln, Germany

[2] Turbine Department, DLR Institute of Propulsion Technology, Deutsches Zentrum für Luft- und Raumfahrt (German Aerospace Center), Göttingen, Germany

[*] michael.schroll@dlr.de, chris.willert@dlr.de

Abstract

We present high-speed particle image velocimetry (HS-PIV) measurements of the compressible flow in a 2d turbine cascade in order to capture the shock–boundary layer interaction (SBLI) that is known adversely affect the heat transfer of cooled turbine stator blades by introducing hot spots along with performance degrading unsteady aerodynamics. Compared to similar HS-PIV measurements in compressor cascade, the present measurements needed to address a number of challenges, such as significant vibration of model and light sheet and unsteady laser flare of the blade's surfaces. In addition, the lack of seeding in the boundary layer (BL), caused by high centrifugal acceleration loads on the tracer particles passing around the leading edge, prevented the acquisition of reliable velocity data in the BL of the blade's suction side. Laser flare in the raw imagery was handled with a proper orthogonal decomposition (POD) based image filtering approach and was able to recover the mean flow field more reliably. However, the data exhibits higher noise levels in the variances which is presumed to be caused by the distortion of particle images during the reconstruction from a limited number of nodes. Estimates of the in-flow turbulence level in the absence of the cascade were obtained by processing 80 kHz imagery with different image strides.

1 Introduction

In modern high-pressure turbine stages, highly loaded airfoils operate in transonic and even supersonic regimes. Normal shocks in the stator throats serve to choke and stabilize the flow. Strong acceleration along the suction side induces a relaminarisation of the boundary layer which affects the formation and extent of shock-induced separation bubbles. In this context the interaction of the shock with boundary layer on the airfoil, (e.g shock–boundary layer interaction (SBLI)) can trigger separation bubbles, abrupt transition zones, and downstream-propagating turbulent wedges. These effects influence local heat transfer, degrade thermal barrier coatings (TBCs), introduce unsteady mechanical loads and ultimately reduces the lifespan of the component. Predicting transition locations is therefore crucial for managing heat transfer and aerodynamic stability. Prior studies (Petersen and Hilfer, 2024) with unsteady temperature sensitive paint (iTSP) show unsteady surface temperature from dominant axial temperature oscillations near 670 Hz. These are linked to the unsteady motion of incident and normal shocks (Fig. 2a).

The unsteady nature of the surface temperature measurements motivates time- and space-resolved measurements of the SBLI phenomena to further validate transition models and define reliable heat margins for next-generation components. To support this, the present high-speed particle image velocimetry (HS-PIV) measurements were performed in a transonic 2d turbine cascade in an effort to capture the unsteady nature of SBLI in transitional boundary layers. In the second part of the investigation HS-PIV measurements were performed on a baseline wind tunnel configuration without the presence of blades or grids to capture upstream conditions. while previous HS-PIV studies on turbine cascades focused on sub-transonic flows, the present work is aimed at resolving the coupled shock–boundary layer dynamics at $Ma_2 = 1.05$, a condition previously studied in detail by (Petersen and Hilfer, 2024).

The campaign spans $Ma_2 = 0.5$ to 1.25, covering engine-relevant Reynolds numbers and builds on previously gained experience in the application of HS-PIV in transonic compressor cascades (see e.g. Klinner et al., 2021, 2024).

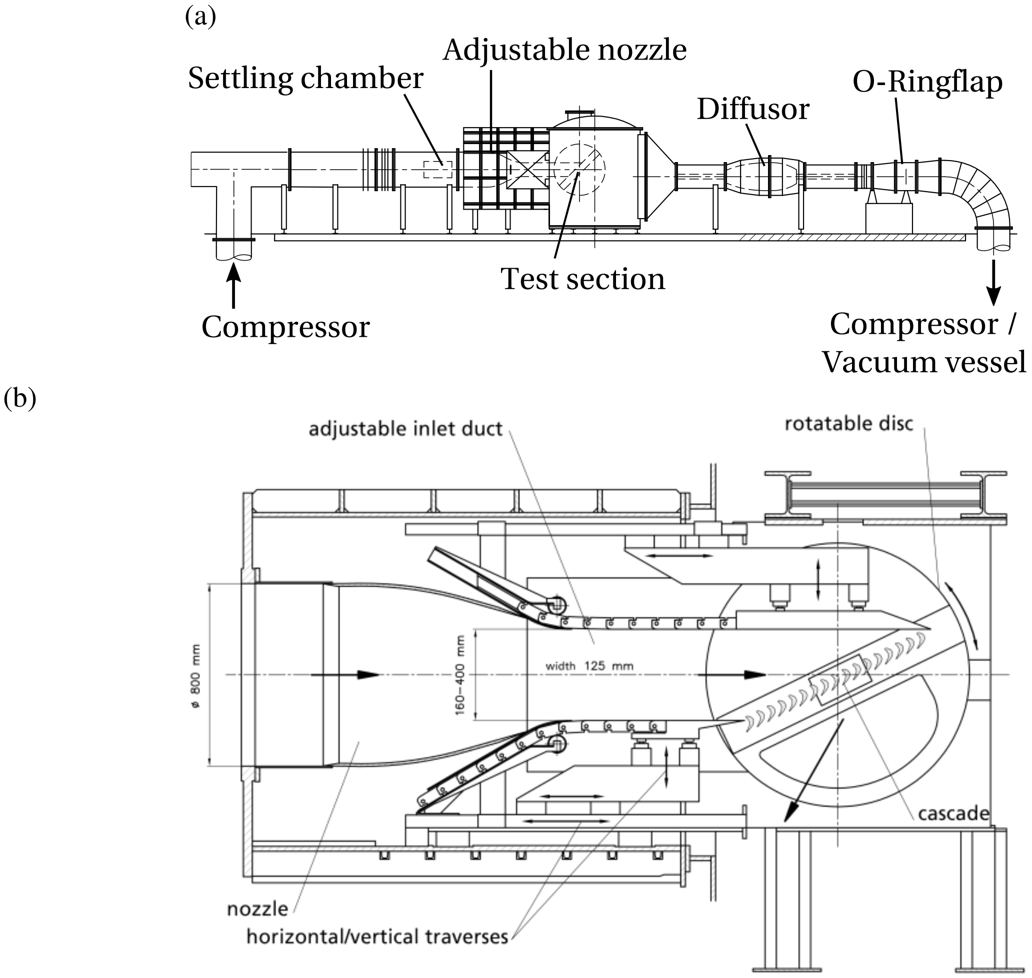

Figure 1: Diagram of the turbine cascade facility of the DLR's Institute of Propulsion Technology in Göttingen. (b) detail of the test section with rotated cascade.

2 Facility and instrumentation

2.1 Turbine cascade facility

The test facility, depicted in Fig. 1(a), is operated at sub-atmospheric conditions and features a turbine cascade that can be rotated to a desired angle of flow incidence as shown in Fig. 1(b). For the present investigation the cascade is rotated to facilitate a parallel, unstaggered flow incidence. The geometric parameters of the investigated configuration are provided in Table 1.

2.2 High-speed PIV setup

For the HS-PIV measurements the light from a dual resonator high-speed laser (Iradion BLIZZ, $2\times 40\,\mathrm{W}$) is introduced into the sub-atmospheric pressure vessel through an optical window and directed into a air-purged light-sheet probe using remotely adjustable mirrors. The probe is placed downstream and below the cascade such that the laser light illuminates the blade's suction side with the high-speed camera imaging the entire passage flow from the throat section to nearly the trailing edge (Fig. 2b). The lasers operate in double-pulse mode at a frequency of 21 kHz synchronized to the high-speed camera (Vision Research T4040) which captured an area of $53\times 19\,\mathrm{mm}^2$ (2048×736 pixel) with a magnification of 26.04 µm/pixel.

Measurements were acquired at four Mach numbers $\mathrm{Ma}_2 = 0.5, 0.9, 1.05, 1.25$, with the condition at $\mathrm{Ma}_2 = 1.05$ of primary interest. Laser pulse delays is the range of $1.12\,\mu\mathrm{s} \leq \Delta t \leq 2.12\,\mu\mathrm{s}$ resulted in particle image displacement around $15.0-20.0$ pixels. Per test-point, 3 runs were acquired each containing five bursts of 1.1 s duration, each consisting of 23 544 images. From a statistics perspective the test-point at $\mathrm{Ma}_2 = 1.05$ comprises approximately 80 000 flow through lengths based on the blade's chord length.

Table 1: Geometric parameters of investigated cascade

Designation	Symbol	Value	Unit
chord length	c	75	mm
span width	h	125	mm
ratio	h/c	1.67	-
axial chord length	c_{ax}	34.67	mm
pitch	t	68.2	mm
throat	A_{min}	14.56	mm
stagger angle	β_s	31.72	°

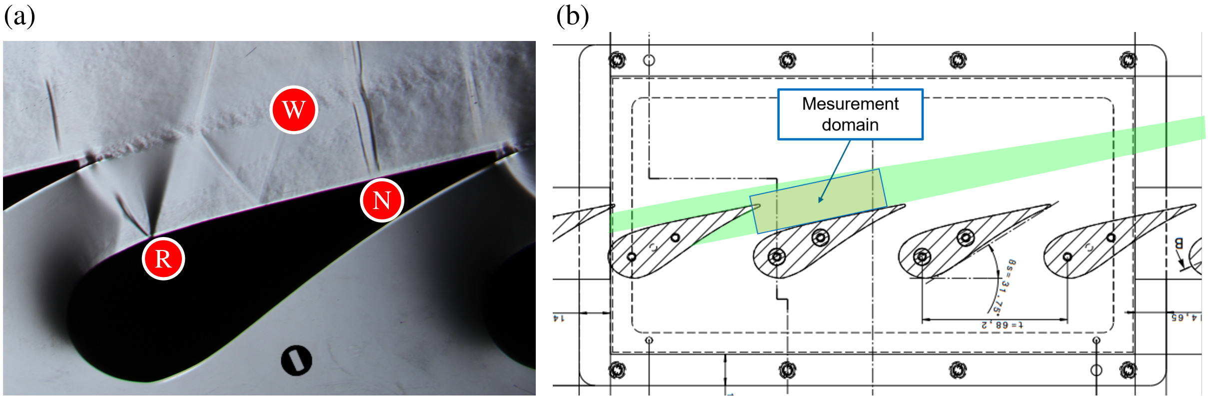

Figure 2: (a): Schlieren image of the cascade flow showing reattachment shock (R), normal shock (N), blade wake (W) (from Petersen, 2021), (b): schematic showing the location of the PIV measurement domain.

To further provide boundary conditions for accompanying large-eddy simulation (LES), the in-flow turbulence is characterized in the absence of the cascade using HS-PIV measurements at a laser pulsing frequency of 80 kHz at a reduced field of view (FOV) of $53 \times 5\,\text{mm}^2$ (2048×192 pixel). For measurements of the in-flow with removed cascade, camera and light-sheet orientation remained unchanged. Both lasers were fired alternately, each running at a repetition rate of 40 kHz. Inflow measurements were conducted at six Mach numbers $\text{Ma}_1 = 0.100, 0.118, 0.137, 0.181, 0.195, 0.222$, with the condition at $\text{Ma}_1 = 1.81$ corresponding approximately to inlet conditions at $\text{Ma}_2 = 1.05$.

3 Results

3.1 Characterization of the in-coming flow

Tracer images of the in-flow were evaluated with different frame separations in order to determine which time-step minimizes measurement uncertainty. The roll-up behavior in the power spectrum is illustrated in Fig. 3a and indicates a varying noise floor depending on the time step (e.g. frame separation). Based on an rms of 0.05 pixel in the displacement detection, the uncertainty in velocity decreases by a factor of 4 up to a time step of 4 and then increases significantly. It can also be seen that the evaluation of odd time steps (laser 1 versus laser 2) is generally accompanied by a higher noise floor, which is attributed to a slight misalignment of the beam overlap as the jitter of the time interval between the two laser pulses is negligible (12 ns rms or 0.02 pixel for subsequent frames). Fig. 3b shows the power spectral density (PSD) resolved over nearly 6 decades for various inlet Mach numbers. The PSDs were estimated using Welch's method using 25 segments of 50% overlap each containing 16384 samples (cut-on at 9.8 Hz) and a cut-off corresponding to the Nyquist frequencies at optimum frame separation of $2-4$ time-steps. The noise floor is less than 1 per mil, making rms values below 1% of the mean axial velocity traceable. When inspecting the axial velocity spectra in Fig. 3b there are peaks around 100 Hz which are damped with increasing Mach number. Despite this peak, the slopes are in agreement with the classical k -5/3 energy decay rate of isotropic inertial-range turbulence.

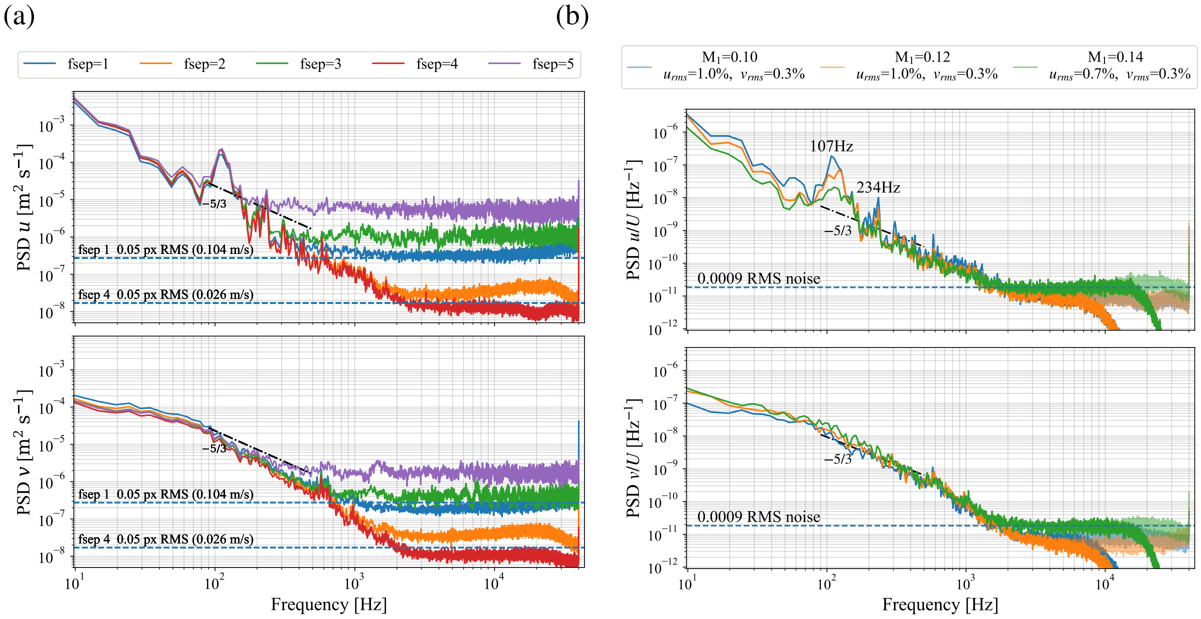

Figure 3: power spectral density (PSD) of both velocity components of the in-coming flow for different frame separations obtained with Fourier-analysis (a): Noise roll-up for various frame separations at $\mathrm{Ma}_1 = 0.1$; (b): PSDs for different inflow-conditions each at optimized frame separation of $2-4$ time-steps.

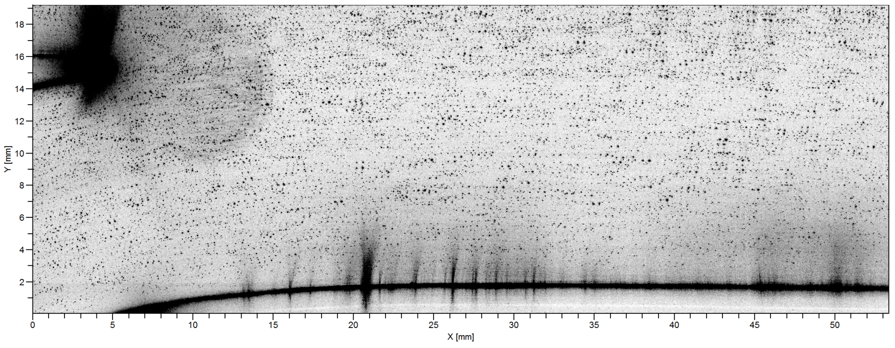

Figure 4: raw overlaid image pair acquired at $\mathrm{Ma}_2 = 1.05$ with a laser pulse delay $\Delta t = 1.2\,\mu\mathrm{s}$ showing strong laser flare and low seeding density near the wall.

3.2 Unsteady flow within the passage

Unlike the previously described incoming flow, the measurements within the cascade were faced with a number of difficulties such as vibrations, laser flare and a near absence of particles in near wall region. Flow induced vibrations of the facility resulted in significant motions in the captured imagery, noticeable by a continuous translation of the profile's laser-illuminated surface. At the same time the non-polished surface of the turbine blade gave rise to irregular laser flare that varied continuously with the motion of the blade (Fig. 4). The absence of tracer particles in the boundary layer region can be attributed to the strong curvature induced acceleration of the flow entering the passage along with a centrifugal force acting on the particles both of which cause the migration of the particles away from the streamline. The following describes various image processing approaches used to reduce the laser flare and vibration related issues.

3.2.1 Image processing approaches

Before the actual PIV evaluation, vibrations of the blade surface were compensated. This is accomplished with a correlation-based algorithm that tracks the relative position of the blade surface for each image by sampling a small rectangular sample region of 20×20 pixel containing the laser flare on the blade suction side at mid-span. To estimate the image shift in each sample, the intensity distribution in each sample region was correlated with several template images of reference blade positions where each template is shifted by a defined amount in the sub-pixel range. The recovered vertical blade displacements have an accuracy of better than 0.2 pixel and are then applied to the raw image data prior to further PIV processing.

The treatment of the time-varying laser flare proved to be more challenging because of the high variability induced by the combination of blade vibration, light sheet motion in spanwise direction and shot-to-shot differences in the laser intensity distribution. If not treated properly the laser flare attenuates the correlation signal of the particles resulting in faulty displacement estimates. Various approaches were chosen to mitigate the influence of laser reflections in the particle images:

- Pre-processing method **A**
  - Subtraction of 50% of mean image intensity separately for laser 1 and laser 2
  - Local contrast normalization filtering aimed at locally homogenizing both the intensity and variance (Sage and Unser, 2001) (parameter settings: $\sigma_1 = 4$, $\sigma_2 = 3$)
- Pre-processing method **B**
  - Subtraction of 50% of mean image intensity separately for laser 1 and laser 2
  - Local contrast normalization using min-max filtering with a kernel size of 11 pixel (Westerweel, 1993),
- Pre-processing method **C**:
  - Random subsets of images grouped into chunks of 200 images (python: `random.shuffle`)
  - POD based background removal (Mendez et al., 2017)
    - ∗ POD of each chunk resulting in 200 modes (python: `sklearn.pca`, full SVD calling standard LAPACK solver)
    - ∗ Reconstruction of particle images from rank r for each chunk (all modes k with $k \geq r$)
    - ∗ The procedure is applied separately to the images of each of the two lasers.

The idea to decompose a particle image into orthogonal modes to enable high-rank reconstruction of particle images by suppressing low-rank laser reflections is not new and was recently described by Mendez et al. (2017). Beyond a certain rank r, the authors assumed that particle images can be distinguished from fluctuating background intensities for a sufficiently large ensemble of images to have the POD modes converged. This implies that fluctuating background intensities vary in phase in several large image regions while variations of particle image intensities are correlated less within the image. For a POD decomposition of particle images Mendez et al. (2017) assumed that from $k > r$ the eigenvalues for a given edge are approximately constant (e.g. $\varepsilon = 0.1\lambda_k$).

On the other hand, for the present set of particle images the singular value spectrum in Fig. 6a) demonstrates, that such a convergence is not feasible. Instead, the decision on the cut-off value of the rank r from which reconstruction is conducted was based on the PIV validation rates in critical image regions such as near the suction side and near the trailing edge of the upper blade. Validation rates for different ranks and exemplary image chunks are shown in Fig. 6b) and reveal an improvement up to $r \approx 20$. Beyond this rank value the validation rate deteriorates rapidly.

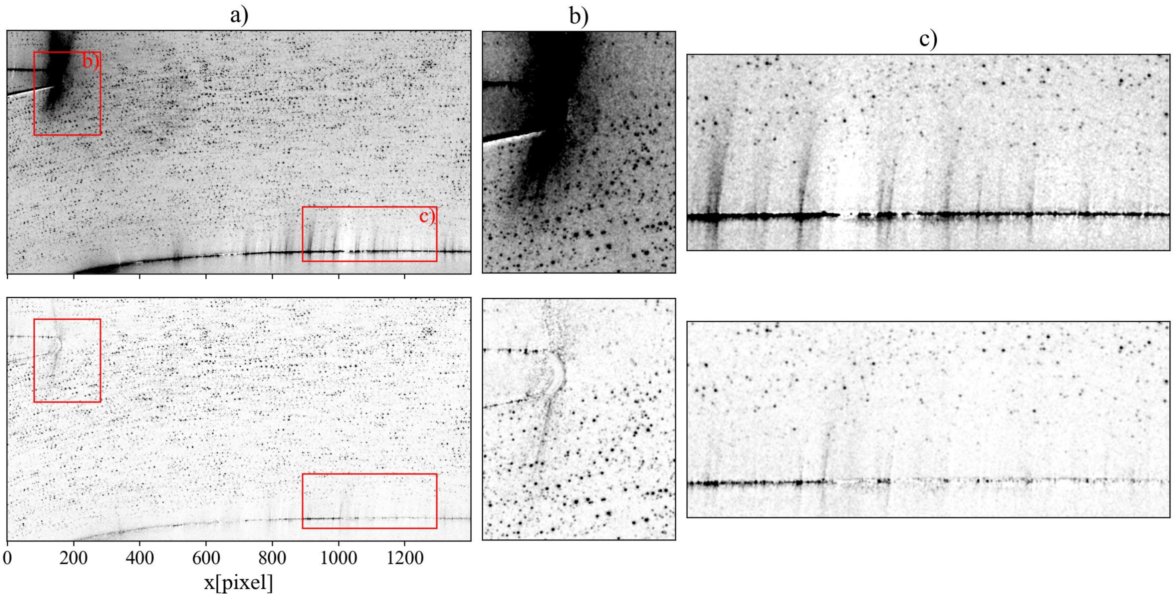

Figure 5: top: image pair at $\mathrm{Ma}_2 = 1.05$ after conventional background subtraction (50% of mean intensity separately for each laser); bottom: background removal using POD based image pre-processing; (b): subregion near the trailing edge; (c) subregion near the suction side

A visual comparison of the effect of the aforementioned three image pre-processing methods on the recovered velocity maps is provided in Fig. 7. Performance-wise the local normalization (method **A**) and min-max filtering (method **B**) yield similar results, with method **A** exhibiting slightly higher noise and outlier levels. The POD-based approach (method **C**) is clearly capable of recovering data in areas where methods **A** and **B** fail and additionally retrieves data in the sparely seeded and flare contaminated region near the wall. Compared to the other two methods, the velocity maps obtained with the POD treated images visually suggests an improved “smoothness” of the velocity field, that is, the velocity maps have a reduced level of noise.

Maps of the mean velocity field at $\mathrm{Ma}_2 = 1.05$ are presented in Fig. 8(a,b) obtained by pre-processing the images either with min-max filtering or with the POD approach. Samples of 48×48 pixel were used for the multiple-pass, grid refining correlation analysis. Globally the filtering has marginal influence on the mean, however, the POD approach extracts more data in regions of high laser flare, such as the suction side and the trailing edge of the blade. Fig. 8(c,d) provide maps of the sum of velocity variances which can be considered a measure of the local turbulent kinetic energy (TKE) although the local (unknown) density ρ is not included in the estimate. In this case the estimates obtained from min-max filtered PIV recordings appears to be less noisy. Distinct features such as the oblique reflected reattachment shock at $y = 12\,\mathrm{mm}$ are attenuated in POD filtered results. It is believed that the POD-based image reconstruction from a limited number of modes distorts the particle images, thereby introducing noise in the displacement estimates.

4 Summary and conclusion

The herein described high-speed particle image velocimetry (HS-PIV) measurements on a transonic turbine stator cascade was originally aimed at capture the flow field dynamics of shock–boundary layer interaction (SBLI). However, the strong leading edge curvature and associated centrifugal forces acting on the tracer particles resulted in insufficient seeding density for reliable velocity estimates in the boundary layer itself. This was further complicated by strong vibrations of blade and camera requiring frame-by-frame image re-alignment. Unsteady laser flare hiding the particle images was handled by a POD-based image filtering method that out-performed conventional image treatment approaches. In spite of these challenges, the unsteady passage flow across a range of Mach numbers could be acquired at 21 kHz with a spatial resolution of $1 \times 1\,\mathrm{mm}^2$ (32×24 pixel sampling). Further analysis of the data will involve spatio-temporal modal decomposition to recover the relevant shock dynamics. The flow field data of the turbine passage are complemented by turbulence level estimates using HS-PIV measurements of the undisturbed flow in the absence of the turbine cascades or other flow blocking obstructions.

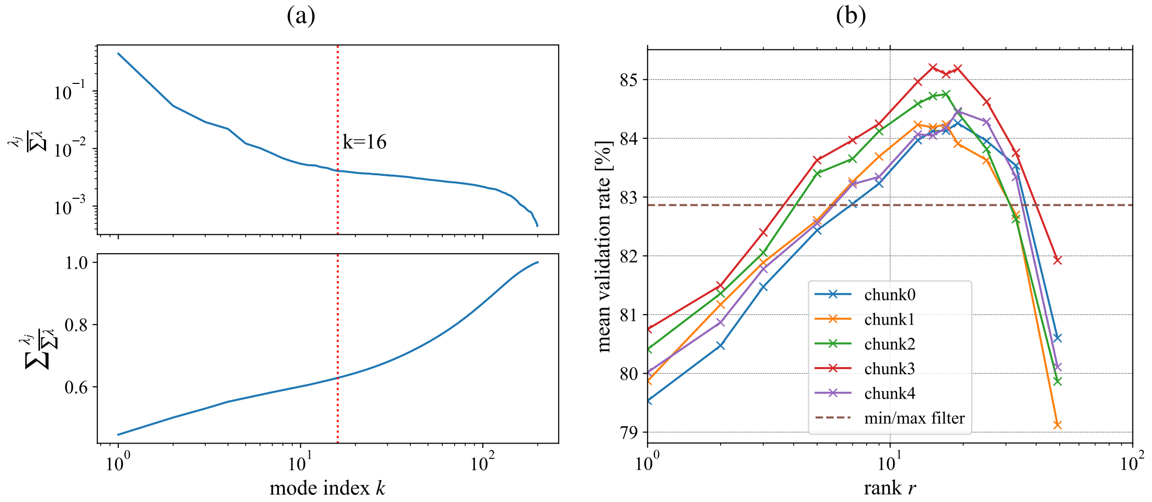

Figure 6: (a): Typical singular value spectrum for a chunk of 200 particle images; (b): rank dependence of PIV validation rate for the POD background removal in 5 random image chunks with 200 image pairs each; dashed line: pre-processing method **B** (min-max filtering).

The collected data serves as a further building block to improve the understanding of SBLI in transitional boundary layers. It sheds light on unsteady phenomena in transonic turbine cascades, supports aerodynamic optimization, enhances predictive models and promotes the design of thermally robust components.

References

Klinner J, Hergt A, Grund S, and Willert C (2021). High-speed piv of shock boundary layer interactions in the transonic buffet flow of a compressor cascade. *Experiments in Fluids* 62:58. doi:10.1007/s00348-021-03145-3. URL `https://doi.org/10.1007/s00348-021-03145-3`

Klinner J, Munoz Lopez E J, Hergt A, and Willert C (2024). The unsteady shock-boundary layer interaction in a compressor cascade – part 1: Measurements with time-resolved PIV. In *Volume 12D: Turbomachinery — Multidisciplinary Design Approaches, Optimization, and Uncertainty Quantification; Radial Turbomachinery Aerodynamics; Unsteady Flows in Turbomachinery*, Turbo Expo, p. V12DT36A008. doi:10.1115/GT2024-124307. URL `https://doi.org/10.1115/GT2024-124307`

Mendez M A, Raiola M, Masullo A, Discetti S, Ianiro A, Theunissen R, and Buchlin J M (2017). POD-based background removal for particle image velocimetry. *Experimental Thermal and Fluid Science* 80:181–192. ISSN 0894-1777. doi:10.1016/j.expthermflusci.2016.08.021. URL `https://www.sciencedirect.com/science/article/pii/S0894177716302266`

Petersen A (2021). *Einfluss pneumatischer Wirbelgeneratoren auf die Effektivität einer gekühlten Hochdruckturbine*. Ph.D. thesis, TU Braunschweig. URL `https://elib.dlr.de/140673/`

Petersen A and Hilfer M (2024). Boundary layer analysis of a transonic high-pressure turbine vane using ultra-fast-response temperature-sensitive paint. *Journal of Turbomachinery* 146(9):091013. ISSN 0889-504X. doi:10.1115/1.4065739. `https://asmedigitalcollection.asme.org/turbomachinery/article-pdf/146/9/091013/7353466/turbo_146_9_091013.pdf`, URL `https://doi.org/10.1115/1.4065739`

Sage D and Unser M (2001). Easy Java programming for teaching image processing. In *Proceedings of the 2001 IEEE International Conference on Image Processing (ICIP'01)*, vol. III, pp. 298–301. Thessaloniki, Greece. URL `https://bigwww.epfl.ch/sage/soft/localnormalization/`

Westerweel J (1993). *Digital Particle Image Velocimetry*. Ph.D. thesis, TU Delft. URL `https://resolver.tudelft.nl/85455914-6629-4421-8c77-27cc44e771ed`

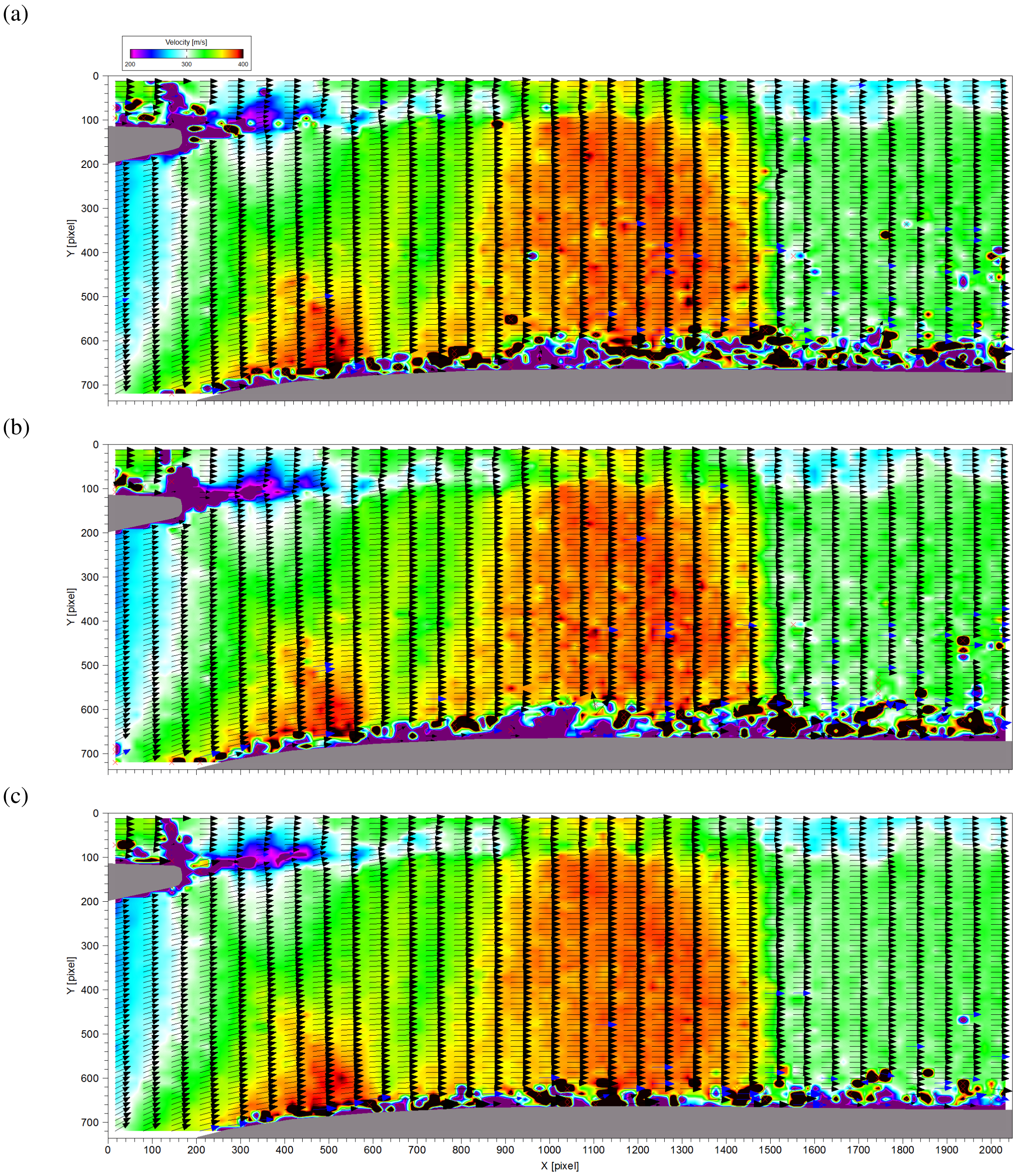

Figure 7: Single velocity map obtained after application of various image pre-processing methods; (a): method **A** (local normalization); (b) method **B** (min-max filtering); (c): method **C** (POD based pre-processing using 200 modes, rank $r = 16$). Displacements are based on samples of 32×24 pixel down-sampled for visibility by 4×1.

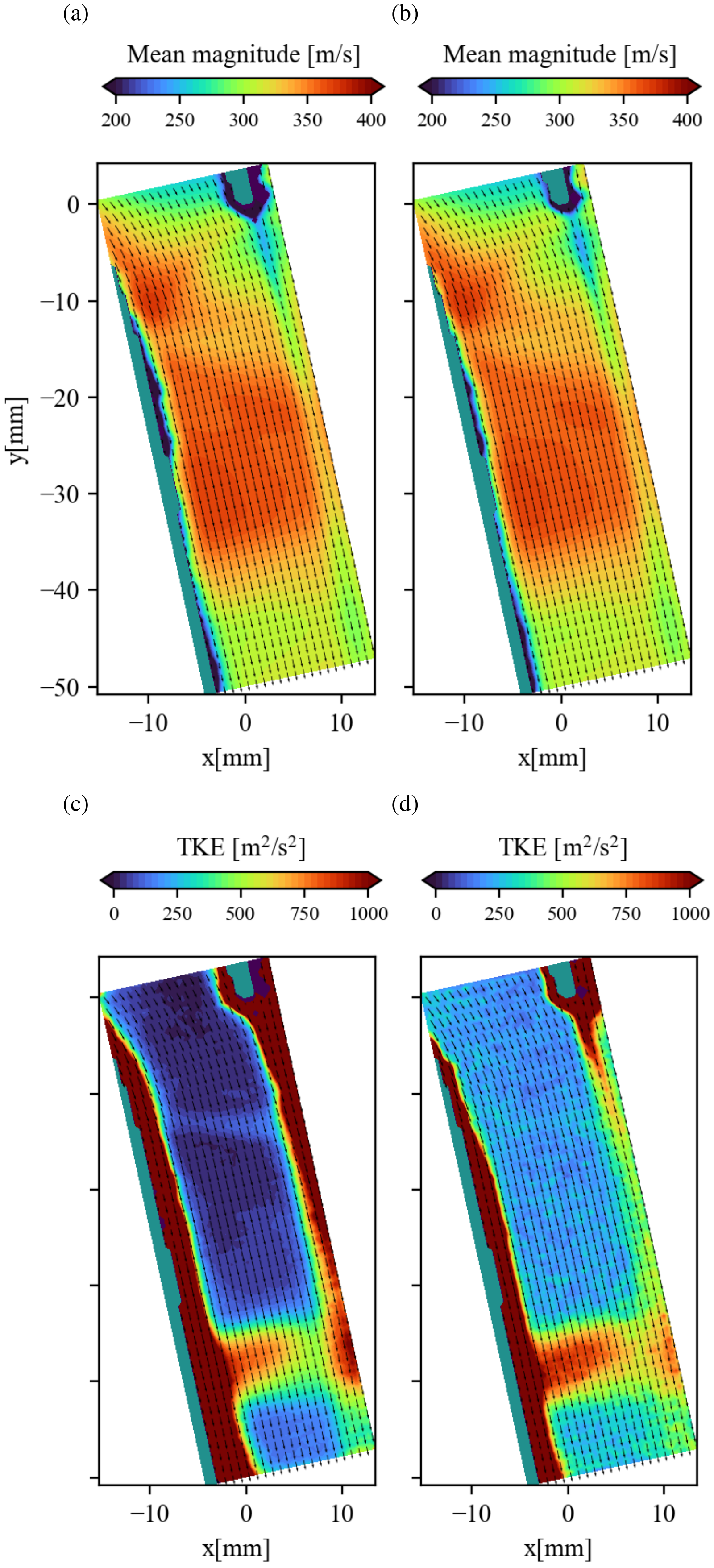

Figure 8: (a): mean velocity fields obtained by applying image pre-processing method **B** (min-max filtering); (b): POD-based image enhancement; (c): TKE estimates by applying method **B**; (d): TKE estimates for POD-based image enhancement.